Letter to the Editor

Detection of C_2H_4 in Neptune from ISO/PHT-S observations

B. Schulz[1]**, Th. Encrenaz**[2]**, B. Bézard**[2]**, P.N. Romani**[3]**, E. Lellouch**[2]**, and S.K. Atreya**[4]

[1] ISO Data Centre, ESA, P.O. Box 50727, E-28080 Madrid, Spain
[2] DESPA, Observatoire de Paris, F-92195 Meudon, France
[3] NASA Goddard Space Flight Center, Code 693.2, Greenbelt, MD 20771, USA
[4] The University of Michigan, Ann Arbor, MI 48109-1243, USA

Abstract. The 6–12 μm spectrum of Neptune has been recorded with the PHT-S instrument of the Infrared Space Observatory (ISO) at a resolution of 0.095 μm. In addition to the emissions of CH_4, CH_3D and C_2H_6 previously identified, the spectrum shows the first firm identification of ethylene C_2H_4. The inferred column density above the 0.2-mbar level is in the range $(1.1–3) \times 10^{14}$ molecules cm^{-2}. To produce this low amount, previous photochemical models invoked rapid mixing between the source and sink regions of C_2H_4. We show that this requirement can be relaxed if recent laboratory measurements of CH_4 photolysis branching ratios at Lyman α are used.

Key words: planets and satellites: general – planets and satellites: individual: Neptune – infrared: solar system

1. Introduction

In the stratospheres of all giant planets, methane (CH_4) photochemistry leads to the formation of many hydrocarbons. Photochemical models have been developed by several authors (e.g. Gladstone et al. 1996 for Jupiter, Moses et al. 1999 for Saturn, Atreya et al. 1991 for Uranus, and Romani et al. 1993 for Neptune) to account for the observations of the detected hydrocarbons (C_2H_2 and C_2H_6) and to predict the abundances of minor species. Among the expected products in significant amount is ethylene (C_2H_4). This compound however was only detected in the northern auroral region of Jupiter, from emission in the ν_7 band at 10.5 μm observed in Voyager/IRIS spectra (Kim et al. 1985). On Neptune, a tentative detection of the same band of ethylene was presented by Orton et al. (1987) from ground-based low-resolution spectral measurements.

Observations with the short-wavelength spectrometer (SWS) of the Infrared Space Observatory (ISO) have led to the detection of several new hydrocarbons in Saturn (C_3H_4, C_4H_2, and CH_3; de Graauw et al. 1997; Bézard et al. 1998) and Neptune (CH_3; Bézard et al. 1999b). In the case of Neptune, the 7–14 μm SWS spectrum, recorded at a spectral resolution of 0.005 μm

has been studied by Bézard (1998). Information was retrieved upon the stratospheric temperature, the CH_4 stratospheric mixing ratio, and the C_2H_2 and C_2H_6 abundance profiles. In the case of C_2H_4, only an upper limit of its stratospheric column abundance (8×10^{14} molecules cm^{-2} above the 0.2–mbar level) was inferred (Bézard et al. 1999a).

We present in this paper the 6–12 μm spectrum of Neptune recorded with another ISO instrument, ISOPHOT, and we report the first firm detection of C_2H_4 on Neptune. Sect. 2 describes the observations and the data reduction. Sect. 3 presents the modelling and the determination of the C_2H_4 abundance. Results are discussed in Sect. 4 and conclusions are presented in Sect. 5.

2. Observations and data reduction

The photometer ISOPHOT (Lemke et al. 1996) of ISO (Kessler et al. 1996) included a subsystem (PHT-S) made of two grating spectrometers operating at 2.5–5 μm (SS) and 6–12 μm (SL) with a spectral resolution of 0.0445 μm and 0.0949 μm respectively (Klaas et al. 1997). The two spectra were simultaneously recorded on the two linear arrays of 64 elements Si:Ga detectors each. The entrance aperture was $24'' \times 24''$.

The PHT-S spectrum of Neptune was recorded on May 8, 1997, between 3:41 UT and 12:29 UT. The diameter of Neptune was then $2.25''$, and the sub-Earth latitude was –30.6°. Twelve pairs of spectra, of 1024 sec integration time each, were successively recorded on and off the source (with the offset position at $5'$ north), in order to subtract the sky background.

The data reduction was performed using the PHT Interactive Analysis software package PIA V7.3.2(e) (Gabriel et al. 1997) together with IDL routines that facilitate individual inspection of the signals and deglitching. The Si:Ga photoconductors, arranged in two arrays of 64 pixels each, exhibit transients of the photocurrent after a flux change. This behavior impacts the deglitching procedure as well as the assignment of flux densities.

The 32 s integration ramps with 128 readouts were divided into 16 subramps. The fitted slopes $s(t)$, being a measure of the photo current, were deglitched automatically using an algorithm
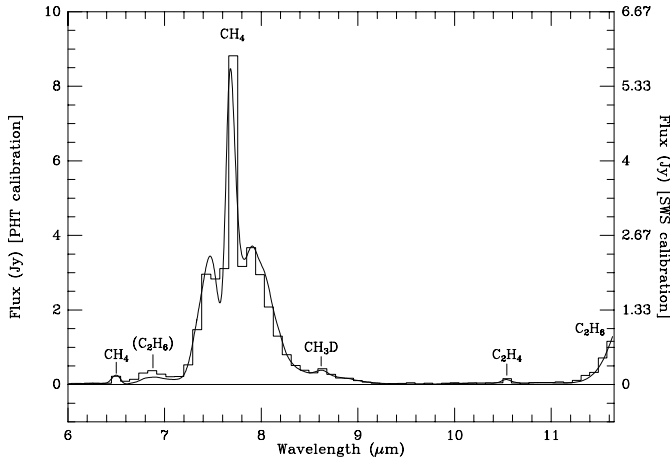
Fig. 1. PHT-S spectrum of Neptune observed in the 6–11.6 μm range. Emission features from CH$_4$, CH$_3$D, C$_2$H$_6$ and C$_2$H$_4$ are clearly detected. The flux scale on the left axis corresponds to the direct PHT-S calibration, that on the right axis to a rescaling of the data by a factor of 0.67 to agree with the SWS observations of the 7.7-μm CH$_4$ band.

that clips all values where $|s(t) - b(t)| > 3.5\sigma$. $b(t)$ are the boxcar smoothed slopes with the smoothing parameter tuned to follow the slow transients of the photo current with time t. σ is calculated as $\sqrt{\sum(s(t) - b(t))^2/(n-1)}$, where n is the number of slopes.

The assignment of flux densities was performed using the new dynamic calibration method (Acosta-Pulido 1999). It is based on the reproducibility of the transient behavior when a given detector pixel is exposed to similar flux levels. The method, which is implemented into PIA, requires the prior subtraction of the exposure time-dependent dark current. The transients also differ from pixel to pixel, so PIA contains a database for all pixels of measured transients with 27 calibration sources, covering most of the accessible flux range. After deriving 12 spectra on source and 12 on the background, we concatenated the pairwise differences within PIA and then averaged each pixel to derive the final flux density.

The uncertainties in the PIA results and propagated statistical errors are usually smaller than the variations due to long-term responsivity changes and transient repeatability. Consistency checks within the database of transients suggest average accuracies of 10 to 15% over all pixels. This is also consistent with results from long-term stability checks (Schulz 1999) which give 10%. Relative uncertainties between fluxes of adjacent detector pixels with similar flux levels are smaller, i.e. closer to the statistical errors. The error in the SED models of the calibration standards is not included and ranges between 3 and 5%.

Fig. 1 shows the PHT-S spectrum of Neptune between 6 and 12 μm. The 1-σ noise level is estimated to about 0.010 Jy at 6–7 μm and 0.020 Jy at 10–11 μm. The spectrum is dominated by the strong ν_4 band of CH$_4$ which peaks at 7.7 μm. CH$_4$ emission is also seen in the Q-branch of the weak ν_2 band at 6.5 μm, observed here for the first time. CH$_3$D is detected at 8.6 μm through its ν_6 band and contributes with its ν_5 band to

the emission at 6.8 μm. The wing of the ν_9 band of C$_2$H$_6$ is visible beyond 11.4 μm. All these emissions above 7 μm were previously detected in the SWS spectrum of Neptune (Bézard 1998). In addition, the PHT-S spectrum of Neptune shows a new emission feature in a single pixel, at 10.5 μm, at a level of 0.1 Jy, i.e. 5 times above the noise level. We attribute this 10.5 μm emission to the Q-branch of the C$_2$H$_4$ ν_7 band, which is centered at 949 cm^{-1} (10.53 μm).

The comparison of the PHT-S and SWS data shows a very good agreement in the shapes of the two spectra, but a difference in the absolute calibration scale by a factor of 1.5, the PHT-S fluxes being higher than the SWS ones. The two scales are indicated on Fig. 1. We have presently no explanation for this discrepancy.

In this paper, we modelled the observations with the "nominal" atmospheric model (methane and temperature profiles) derived by Bézard (1998) from an analysis of the SWS spectrum between 7 and 14 μm (see Sect. 3). The C$_2$H$_2$ and C$_2$H$_6$ abundances inferred from this model were in very good agreement with previous results from Voyager data (Bézard et al. 1991) and ground-based infrared measurements (Orton et al. 1987). For consistency, we used here the SWS calibration of the PHT-S data to infer the "nominal" C$_2$H$_4$ abundance, but we took into account the difference in the two instrument calibrations in the error analysis.

3. Radiative transfer analysis

Synthetic spectra were generated from a line-by-line radiative transfer program that includes the H$_2$-He collision-induced absorption and molecular opacity from CH$_4$, CH$_3$D, C$_2$H$_6$, and C$_2$H$_4$. Line parameters come from the 1997 spectroscopic Geisa databank (Jacquinet-Husson et al. 1997). We used the same temperature profile as in Bézard (1998) and Bézard et al. (1999b). C$_2$H$_4$ spectral calculations were carried out assuming LTE at all atmospheric levels.

To derive constraints on the C$_2$H$_4$ stratospheric column abundance, we proceeded as did Bézard et al. in their analysis of the methyl radical emission. We considered vertical profiles derived from photochemical calculations, allowing for the uncertainty in the photochemical scheme (Profiles 1–5 in Table 1) and in the eddy mixing profile (Profiles 6–7) (see Sect. 4). To determine the C$_2$H$_4$ abundance implied by the observations, we then multiplied each test profile by a constant factor that allowed us to best reproduce the intensity of the observed 10.5-μm emission in a least-squares sense. We found column densities for these rescaled profiles in the range 1.7–2.2×10^{14} molecules cm^{-2} down to the 0.2-mbar level (Table 1). The C$_2$H$_4$ abundance below this level does not contribute significantly to the emission, being located at colder levels in the stratosphere.

The spectrum generated with our nominal model (Profile 5 for C$_2$H$_4$) is shown in Fig. 1 in the whole range 6–11.6 μm. The discrepancy between the synthetic and observed spectra around 6.8 μm may be due to the presence of the ν_8 band of C$_2$H$_6$. This band was not included in the calculations as no line compilation exists in the usual spectral databanks. In the other regions, the

Table 1. Comparison of photochemical models to ISO observations

Model	K_h (cm^2 s^{-1})	CH$_4$ branching ratios at Ly α	H + C$_2$H$_4$ rate coefficient	Model C$_2$H$_4$ (molecules cm^{-2} at 0.2 mbar)	Scaled C$_2$H$_4$[a]
1	1×10^7	Romani (1996)	Lightfoot & Pilling (1987) nominal	8.8×10^{14}	1.9×10^{14}
2	1×10^7	Heck et al. (1996)	Lightfoot & Pilling (1987) nominal	4.3×10^{14}	1.9×10^{14}
3	1×10^7	Smith & Raulin (1999)	Lightfoot & Pilling (1987) nominal	3.0×10^{14}	1.9×10^{14}
4	1×10^7	Smith & Raulin (1999)	Lightfoot & Pilling (1987) fast	2.2×10^{14}	1.8×10^{14}
5	1×10^7	Smith & Raulin (1999)	Baulch et al. (1994)	1.6×10^{14}	1.7×10^{14}
6	1×10^6	Smith & Raulin (1999)	Lightfoot & Pilling (1987) nominal	2.2×10^{14}	2.2×10^{14}
7	5×10^7	Smith & Raulin (1999)	Lightfoot & Pilling (1987) nominal	3.3×10^{14}	1.8×10^{14}

[a] Needed to reproduce the C_2H_4 emission intensity

agreement is quite satisfactory. Spectra incorporating various vertical profiles of C_2H_4 (Profiles 1–5, Fig. 2) are shown in Fig. 3 (see Sect. 4 for a full description of the profiles).

Our nominal value for the inferred column density is 1.7×10^{14} molecules cm^{-2}, using the rescaled profile 5. Uncertainties arise from the noise level ($\pm20\%$), the flux calibration of the ISO spectrum, the model temperature profile, and the C_2H_4 vertical profile. For the flux calibration uncertainty, we assumed a $^{+50}_{-30}\%$ error interval that includes the PHT-S flux scale. Uncertainties from the temperature profile were estimated using the extreme "cool" and "warm" profiles from Bézard et al. (1999b). A $^{+20}_{-15}\%$ error range was then obtained. Finally the uncertainty due to the C_2H_4 height profile is $^{+25}_{-5}\%$ (Table 1). Combining the above error bars, we conclude that the C_2H_4 column density above the 0.2-mbar level is in the range $(1.1–3)\times10^{14}$ molecules cm^{-2}.

4. Comparison with photochemical models

Photochemical calculations were carried out with a one-dimensional model as in Bézard et al. (1999b). The model has been most recently described in Bishop et al. (1997). Chemical reactions and kinetic rates included in the modeling are listed in Table 3 of Bishop et al. with minor updates since then, except for the methane photolysis branching ratios at Lyman α and the rate coefficient for $C_2H_4 + H + M \rightarrow C_2H_5 + M$, which are both discussed below. Photolysis rates are calculated for disk-averaged conditions, and account for both solar irradiance and the Lyman α skyglow from the local interstellar medium. Solar minimum conditions, representative of the time of the ISO observations, were used, because the chemical lifetime of C_2H_4 was found to be shorter than the solar cycle. We used a CH$_4$ mole fraction equal to 1.4×10^{-3} in the lower stratosphere as favored by observations of the ν_4 band of methane by ISO (Bézard 1998). The model incorporates a downward flux of atomic hydrogen at the upper boundary equal to 4×10^7 cm^{-2} s^{-1}, representing H production from solar EUV at solar minimum.

We used as "nominal" an eddy mixing coefficient, K, proportional to the atmospheric number density n to the –0.6 power, and equal to $K_h = 10^7$ cm^2 s^{-1} at the methane homopause. This type of K profile was shown to be compatible with the ISO observations of CH$_3$ if the low pressure rate coefficient for the methyl self-reaction was between that of Slagle et al. (1988)
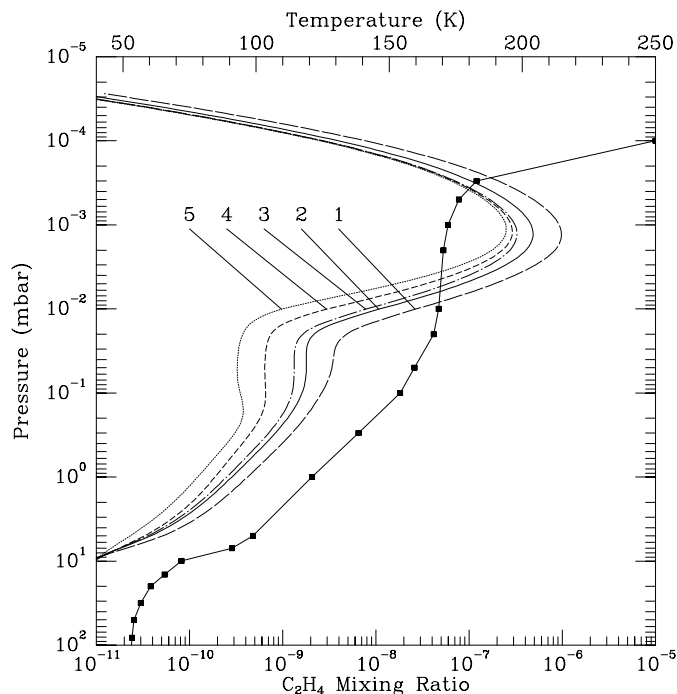

Fig. 2. Temperature-pressure profile used in the radiative transfer analysis (solid line with dots, top axis) and calculated C_2H_4 profiles. Three different CH$_4$ photolysis branching ratios at Lyman α were first used: Romani (1996) [long-dashed line], Heck et al. (1996) [dash-dot line], Smith and Raulin (1999) [solid line], all with the nominal value of the reaction rate coefficient for H + C_2H_4 from Lightfoot and Pilling (1987). Different expressions of the reaction rate coefficient of H + C_2H_4 were also considered: Lightfoot and Pilling's (1987) nominal expression [solid line], Lightfoot and Pilling's fast rate [short-dashed line], Baulch et al. (1994) [dotted line], all with CH$_4$ photolysis branching ratios from Smith and Raulin (1999).

and Macpherson et al. (1985). Following Bézard et al. (1999b), we also varied the K profile, considering constraints from other observations of Neptune hydrocarbons (Bishop et al. 1997).

Ethylene photochemistry is similar to that of the methyl radical CH$_3$ (see Bézard et al. 1999b). It has a source high in the stratosphere (3 to 0.3 μbar region) from methane photolysis, a three-body sink low in the stratosphere (0.1 to 1 mbar region), and transport connecting the two. Methylidyne (CH) is directly produced from methane photolysis as is methyl, and yields ethy-

lene via CH + CH_4. Triplet methylene ($^3CH_2$), another product of methane photolysis, also leads to C_2H_4 formation. The net effect is that C_2H_4 production is sensitive to the sum of the photolysis pathways that yield either $^3CH_2$ or CH. The dominant sink for ethylene is, in the lower stratosphere, the three-body reaction $C_2H_4 + H + M \rightarrow C_2H_5 + M$. The C_2H_4 column density is proportional to its production rate but inversely proportional to the loss rate coefficient and to the transport rate between the source and the sink.

The methane photolysis rate is dominated by the flux at Lyman α. Unfortunately, the branching ratios for the possible pathways at Lyman α are still not known. Furthermore, there are disagreements among the laboratory experiments about the relative importance of the different pathways and the quantum yield of H and H_2 in methane photolysis (Smith and Raulin 1999, Brownsword et al. 1997, Heck et al. 1996, Mordaunt et al. 1993). We first used the same branching ratios as in Romani (1996) (Profile 1 in Fig. 2). These branching ratios are based upon the work of Mordaunt et al. (1993) and previous work. As can be seen in Fig. 3, this produces too large a column density of C_2H_4 to be compatible with the observations. We next tried the branching ratios suggested by Heck et al. (1996) (Profile 2). The main difference with those of Romani (1996) is that the production of $^3CH_2 + 2H$ is reduced from 0.21 to zero while the production of $CH_3 + H$ is increased by a similar amount. The column density of C_2H_4 decreases, but not enough to match the observations (see Table 1 and Fig. 3). Lastly we used the branching ratios of Smith and Raulin (1999) (Profile 3), which are very similar to those of Brownsword et al. (1997). With respect to ethylene formation, the major difference between these branching ratios and those of Heck et al. (1996) is a reduction in the branching ratio to form $CH + H_2 + H$ from 0.11 to 0.06. The modelled C_2H_4 column density is now close to the value derived from the observations.

The predicted C_2H_4 emission is still slightly too high, although the branching ratios of Smith and Raulin result in the lowest model predicted C_2H_4 column density of all that we tried. We next investigated the loss processes for ethylene. We used the "fast" rate coefficient for $H + C_2H_4$ from Lightfoot and Pilling (1987) (the largest possible rate coefficient within their reported error bars) (Profile 4). Using this rate coefficient with the Smith and Raulin branching ratios, the modelled C_2H_4 profile now yields the correct abundance to reproduce the observed emission within the noise level (see Table 1, Figs. 2–3). It can be noted that the rate coefficient expression suggested by Baulch et al. (1994) for this reaction is faster than the "fast" Lightfoot and Pilling (1987) value. It results in a predicted C_2H_4 emission still consistent with the observations (Profile 5).

It is also possible to reduce the C_2H_4 column density by changing K. A first way is to keep the same functional form, $K{\sim}n^{-0.6}$, but to decrease its value at the methane homopause. Methane photolysis then occurs at higher number densities, closer to the C_2H_4 loss region. To reproduce the C_2H_4 emission feature with the Smith and Raulin (1999) branching ratios K must be lowered to $5{\times}10^6\,cm^2\,s^{-1}$ at the methane homopause, but with the Romani (1996) branching ratios K must
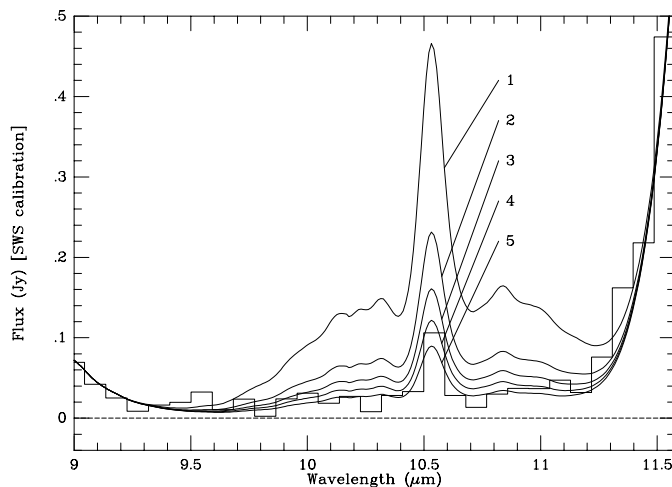

Fig. 3. Synthetic spectra calculated with the C_2H_4 profiles 1–5 of Table 1 (solid lines), displayed in Fig. 2, are compared with the PHT-S spectrum in the region of the ν_7 ethylene band (histograms).

be decreased below $10^6\,cm^2\,s^{-1}$. The former value is within the bounds permitted by the ISO/SWS CH_3 observations while the latter is not (Bézard et al. 1999b). A second way is to alter the form of K to increase the downward transport of C_2H_4 from its source to sink. This was done previously by Romani et al. (1993) and Bishop et al. (1997). They found that the model predicted C_2H_4 with $K{\sim}n^{-0.6}$ was too high for the Voyager UVIS solar occultation light curves (note that these papers were prior to Brownsword et al. (1997) and thus had high C_2H_4 production). They solved the problem by increasing the transport rate between the μbar and mbar region (type "B" eddy profile in Romani et al. 1993) and using the fast rate coefficient for $H + C_2H_4$ from Lightfoot and Pilling. With this combination of transport and chemistry, the C_2H_4 column density is now within the range allowed by ISOPHOT although at the upper bounds.

5. Summary and conclusions

The PHT-S detection of the C_2H_4 ν_7 band on Neptune implies a column density equal to $1.7^{+1.3}_{-0.6}\times10^{14}$ molecules cm^{-2}. This result is fully consistent with the upper limit of 8×10^{14} molecules cm^{-2} reported by Bézard et al. (1999a) from ISO-SWS observations. Orton et al.'s (1987) observations of Neptune at a resolution of $0.23\,\mu m$ showed enhanced emission around $10.5\,\mu m$ that was attributed to C_2H_4. Their reported brightness temperature at $10.5\,\mu m$ corresponds to a 0.06 Jy flux ($\pm20\%$), in good agreement with the PHT-S spectrum which yields a value of 0.09 (PHT calibration) or 0.06 Jy (SWS calibration) after convolution at 0.23-μm resolution.

For the photochemical model to reproduce both the ISO CH_3 and C_2H_4 emission features with $K{\sim}n^{-0.6}$, the CH_4 photolysis branching ratios at Lyman α must be similar to those proposed by Brownsword et al. (1997) and Smith and Raulin (1999). Furthermore, if $K_h = 10^7\,cm^2\,s^{-1}$, the rate coefficient for $H + C_2H_4$ must be near the "fast" value of Lightfoot and Pilling (1987).

It is also possible to invoke rapid transport between the μbar and mbar region (type "B" K profile from Romani et al. 1993). In this case, the CH_4 photolysis branching ratios at Lyman α that lead to C_2H_4 production must be increased above those proposed by Brownsword et al. (1997) and Smith and Raulin (1999). However, a fast rate for $H + C_2H_4$ is still needed.

In summary, previous photochemical models required rapid transport and a fast sink for C_2H_4 to reproduce observations. Now the new laboratory measurements of CH_4 photolysis branching ratios at Lyman α allow us to relax that requirement. The need for laboratory measurements mentioned by Romani et al. (1993) – the CH_4 branching ratios at Lyman α, and the rate coefficient of $H + C_2H_4$ at low temperatures and pressures – is still present.

References

Acosta-Pulido J., 1999, Dynamic Calibration of ISOPHOT-S, IDC technical note, in preparation

Atreya S.K., Sandel B.R., Romani P.N., 1991, Photochemistry and vertical mixing. In: Bergstralh J.T., Miner E.D., Matthews M.S. (eds) Uranus. Univ. Arizona Press, Tucson, p.110

Baulch D.L., Cobos C.J., Cox R.A., et al., 1994, J. Phys. Chem. Ref. Data 23, 847

Bézard B., 1998, Ann. Geophys. 16 (Suppl. III), C1037

Bézard B., Romani P.N., Conrath B.J., Maguire W.C., 1991, JGR 96, 18961

Bézard B., Feuchtgruber H., Moses J.I., Encrenaz T., 1998, A&A 334, L41

Bézard B., Feuchtgruber H., Encrenaz T., 1999a, ESA-SP 427, 153

Bézard B., Romani P.N., Feuchtgruber H., Encrenaz T., 1999b, ApJ 515, 868

Bishop J., Romani P.N., Atreya S.K., 1997, Plan. Space Sci. 46, 1

Brownsword R.A., Hillenkamp M., Laurent T., Vasta R.K., Volpp H.R., Wolfrum J., 1997, Chem. Phys. Lett. 266, 259

de Graauw Th., Feuchtgruber H., Bézard B., et al., 1997, A&A 321, L13

Gabriel C., et al., 1997, In: Hunt G., Payne H.E. (eds) Proc. ADASS VI conference, ASP Conf. Ser. 125, p.108

Gladstone G.R., Allen M., Yung Y.L., 1996, Icarus 119, 1

Heck A.J.R., Zare R.N., Chandler D.W., 1996, J. Chem. Phys. 104, 4019

Jacquinet-Husson N., Arié E., Ballard J., et al., 1997, JQSRT 62, 205

Kim S.J., Caldwell J., Rivolo A. R., Wagener R., Orton G. S., 1985, Icarus 64, 233

Kessler M.F., Steinz J.A., Anderegg M.E., et al., 1996, A&A 315, L27

Klaas U., Acosta-Pulido J.A., Ábrahám P., et al., 1997, ESA SP-419, 113

Lemke D., Klaas U., et al., 1996 A&A 315, L64

Lightfoot P.D., Pilling M.J., 1987, J. Phys. Chem. 91, 3373

MacPherson M.T., Pilling M.J., Smith M.J.C., 1985, J. Phys. Chem. 89, 2268

Mordaunt D.H., Lambert I.R., Morley G.P., et al., 1993, J. Chem. Phys. 98, 2054

Moses J., Bézard B., Lellouch E., Gladstone G.R., Feuchtgruber H., Allen M., 1999, Icarus, submitted

Orton G., Aitken D.K., Smith C., Roche P., Caldwell J., Snyder R., 1987, Icarus 70, 1

Romani P.N., 1996, Icarus 122, 233

Romani P.N., Bishop J., Bézard B., Atreya S.K., 1993, Icarus 106, 442

Schulz B., 1999, Long Term Responsivity Stability of ISOPHOT-S, IDC technical note

Slagle I.R., Gutman D., Davies J.W., Pilling M.J., 1988, J. Phys. Chem. 92, 2455

Smith N.S., Raulin F., 1999, JGR 104, 1873